J Therm Anal Calorim (2009) 98:449–455
DOI 10.1007/s10973-009-0300-4

Studies on the thermal decomposition kinetics and mechanism of ammonium niobium oxalate

T. T. Su · Y. C. Zhai · H. Jiang · H. Gong

Received: 17 November 2008 / Accepted: 26 January 2009 / Published online: 28 July 2009

Abstract Ammonium niobium oxalate was prepared and characterized by elemental analysis, XRD and FTIR spectroscopy analysis, which confirmed that the molecular formula of the complex is $NH_4(NbO(C_2O_4)_2(H_2O)_2)(H_2O)_3$. Dynamic TG analysis under air was used to investigate the thermal decomposition process of synthetic ammonium niobium oxalate. It shows that the thermal decomposition occurs in three stages and the corresponding apparent activation energies were calculated with the Ozawa–Flynn–Wall and the Friedman methods. The most probable kinetic models of the first two steps decomposition of the complex have been estimated by Coats–Redfern integral and the Achar–Bridly–Sharp differential methods.

Keywords Apparent activation energy · Kinetic model · Thermal decomposition

Introduction

Niobium chemistry is not widely known despite increasing interest in the application of niobium compounds within many fields. Niobium materials are presently of great interest in heterogeneous catalysis where they are used as catalyst active ingredient, carrier or auxiliary agent [1]. In these niobium-contain materials, the excellent water-soluble ammonium niobium oxalate is the optimum selection [2]. It is fairly inexpensive and does not suffer from the drawbacks of halides or orthoniobates [3]. However, niobium compounds exhibit special properties, which are not shown by the compounds of neighboring elements of niobium in the periodic table. Some prosperities of ammonium niobium oxalate, such as thermal stability or decomposition mechanism, are very important for the preparation of a good niobium-containing catalyst [4]. Thus, it is desirable to understand the decomposition process as well as the factors influencing the morphology of the decomposition products.

Thermal decompositions of metal oxalates have contributed to establishing the theoretical concepts of solid-state decomposition. The decomposition of transition metal oxalates has been the subject of numerous studies, e.g. Fe [5, 6], Cu [7], Ni, Co and Mn oxalates [8]. Some studies were conducted using the isothermal technique [5–7], while others were performed using non-isothermal methods [9]. Several articles were concerned with the mechanistic aspects and kinetics of the nucleation and growth behavior, including microscopic examination. Boldyrev et al. [10] concluded that the first step in the decomposition of all oxalates is the cleavage of the C–C bond in the anion $C_2O_4^{2-}$. The residual solid product may be the metal oxide or the metal depending on the electropositivity of the cation [11].

In the present study, ammonium niobium oxalate has been synthesized and characterized by elemental analysis, X-ray powder diffraction (XRD) analysis, FTIR spectroscopy and thermogravimetric (TG) analysis. Kinetic methods, such as the Ozawa–Flynn–Wall [12] (OFW, utilizing the dependence lg of heating rate vs. $1/T$) and Friedman [13] (FR, utilizing the dependence $\ln d\alpha/dt$ vs. $1/T$) were used in this study to evaluate the apparent activation energy. The most probable kinetic model of thermal

T. T. Su · Y. C. Zhai
College of Materials & Metallurgy, Northeastern University, 110005 Shenyang, People's Republic of China

T. T. Su · H. Jiang (✉) · H. Gong
Liaoning Shihua University, 113001 Fushun, People's Republic of China
e-mail: hjiang78@hotmail.com

decomposition of the compound has been suggested according to Coats–Redfern (C–R) [14] integral method and Achar–Bridly–Sharp (ABS) [15] differential method.

Experimental

Sample preparation

All materials were commercially available and were of analytical grade.

The method of preparation of ammonium niobium oxalate is similar to CN1935772 [2]. Oxalic acid (200 g) was added to 250 mL of water under stirring and the oxalic acid solution with the concentration of 0.48 g L^{-1} was obtained. Niobic acid (100 g, water content: 25%) was added after the solution was heated to 100 °C. Ammonium oxalate (10 g) was added after reacting for 25 min at 100 °C. Stop heating until ammonium oxalate was completely dissolved. The solution was vaporized to the concentration of 1.5 g L^{-1} and then cooled to room temperature, causing the desired ammonium niobium oxalate to precipitate out of the solution. The precipitate was filtered off and died at 150 °C. Recrystallization from water yielded the pure ammonium niobium oxalate.

Elemental analysis for $C_4H_{14}NO_{14}Nb$ found (%): C, 12.01; H, 3.45; N, 3.83; calc. (%): C, 12.22; H, 3.56; N, 3.56. The content of niobium was determined by thermogravimetry analysis.

Methods

Elemental analysis was carried on Perkin–Elmer PE-2400 II Series CHNS/O analyzer.

X-ray power diffraction patterns were obtained with a D/max-RB diffractometer in the 2θ range using graphit-monochromated Cu$K\alpha$ radiation (40 kV, 100 mA). The step scan mode was performed with a step width of 0.02°, at a rate of 4° (2θ) per min.

FTIR spectrum was obtained in KBr discs on a Perkin–Elmer Spectrum GX. Sixteen scans were co-added with a resolution of 4 cm^{-1}, in the range of 4,000–400 cm^{-1}.

Thermal degradation kinetics studies were carried out on a Perkin–Elmer Pyris 1 TGA. The atmosphere was air with a flow rate of 20 ml min^{-1}. The selected heating rates were 1, 2, 5, 10 and 20 K min^{-1}. The sample mass is about 2.2 ± 0.02 mg and temperature range is from 30 to 700 °C. TG analysis of niobic acid ($Nb_2O_5{\cdot}2H_2O$) was performed at 20 K min^{-1} under air with 2.219 mg sample. To verify the reproducibility of obtained mass loss curves, two sample runs were performed under the same experimental conditions for each sample at each selected heating rate first. The approximate overlapping of two mass loss curves from two separate test runs was considered as reasonable agreement; otherwise, another two runs were performed then to determine which one should be chosen.

Results and discussion

X-ray diffraction analysis

Figure 1 shows the XRD pattern of the synthetic ammonium niobium oxalate. The XRD pattern matched well with the standard data complied in the PDF card no. 83-1993 of ammonium niobium oxide oxalate hydrate ($NH_4(NbO(C_2O_4)_2(H_2O)_2)(H_2O)_3$), which agree with the elemental analysis results of the synthetic ammonium niobium oxalate. Therefore, the stoichiometry of the complex has been established as $NH_4(NbO(C_2O_4)_2(H_2O)_2)(H_2O)_3$. The molecular structure is exhibited in Fig. 2.

FTIR spectrum of ammonium niobium oxalate

The main infrared bands for the synthetic ammonium niobium oxalate are summarized in Table 1.

Thermogravimetric analysis

Figure 3 shows TG curves of ammonium niobium oxalate (a) and niobic acid (b) ($Nb_2O_5{\cdot}2H_2O$) at heating rate of

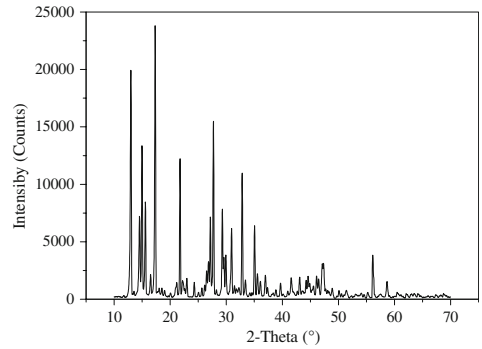

Fig. 1 The XRD pattern of the synthetic ammonium niobium oxalate

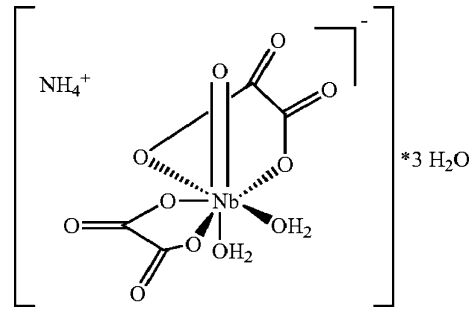

Fig. 2 Molecular structure of the synthetic ammonium niobium oxalate

Table 1 Main infrared bands for the synthetic ammonium niobium oxalate

Bands (cm^{-1})	$NH_4(NbO(C_2O_4)_2(H_2O)_2)(H_2O)_3$
ν_{O-H}	3,588 (m), 3,438 (m)
ν_{N-H}	3,178 (m), 3,028 (m)
δ_{O-H}	1,626 (m)
δ_{N-H}	1,397 (s)
$\nu_{C=O}$	1,717 (s)
$\delta_{(COO)}^{-}$	804 (m)
ν_{Nb-O}	547 (m), 495 (m)
ν_{C-O}	1,226 (m)
$\nu_{Nb=O}$	947 (s), 910 (m)

s strong, *m* medium

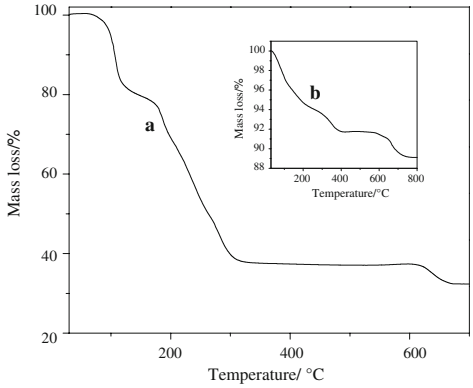

Fig. 3 TG curves of ammonium niobium oxalate (a) and niobic acid (b) at 20 K min^{-1} under air atmosphere

20 K min^{-1} under air environment. And the FTIR spectra of ammonium niobium oxalate in different decomposition temperature are exhibited in Fig. 4.

It shows from Fig. 3a that the decomposition of the synthetic complex proceeds through three steps with TG curves closely corresponds to the theoretical mass loss.

The 21.59% mass loss between 30 and 145 °C is attributed to the dehydration of ammonium niobium oxalate and formation of anhydrous complex. It also can be conformed by the disappearing of the absorption peaks of 3588, 3438 and 1626 cm^{-1} (Fig. 4). The 38.81% mass loss between 145 and 330 °C is due to the decomposition of oxalate ligands and the release of ammonia, which produce $Nb_2O_5{\cdot}H_2O$. The absorption peaks of oxalate disappear at a temperature above 330 °C. TG curve shows the second step is consecutive with the first one. Therefore, there is less carbon dioxide at about 145 °C, which adsorbs on amorphous powder phase niobic acid. The third step occurs at about 560 °C with a mass loss of 4.98% due to the formation of anhydrous Nb_2O_5 and the adsorbed CO_2 was deadsorbed. At this stage, niobic acid undergoes a transition from amorphous to hexagonal or orthorhombic phase

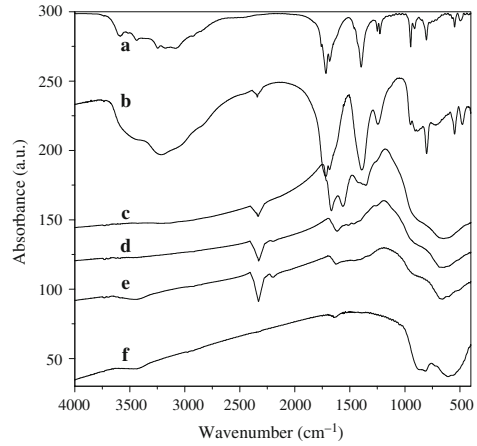

Fig. 4 The FTIR spectra in different decomposition temperature: a-original sample; b-145 °C; c-240 °C; d-330 °C; e-500 °C; f-700 °C

(TT or T, respectively) crystallization. This conclusion can be confirmed by the thermal decomposition process of niobic acid (Fig. 3b). They have the same temperature range of mass loss. Furthermore, as shown in Fig. 4, at 500 °C, niobic acid shows three broad bands: ~900, 655, and a small shoulder at 511 cm^{-1}. These bands can be assigned to Nb=O in highly distorted NbO_6 groups, symmetric stretching of the niobia polyhedra, and ν(Nb–O) in slightly distorted NbO_6 octahedra, respectively. At 700 °C, Nb_2O_5 shows finer characteristics in the same spectral region. There is a large band with a maximum of ~860, three bands at 722, 610, and 566, and a band at 500 cm^{-1}, which are attributed to the main above-mentioned vibrations [16]. This process also can be followed up by XRD patterns at different temperatures as seen in literatures [1, 16].

Kinetic studies

The decomposition kinetics study is important to know the decomposition mechanism, rate of reaction, reaction parameters and to predict the products distribution. This in turn helps in proper selection of reactor, optimization of the reactor design and operating conditions [17].

Model-free estimation of activation energy

All kinetic analyses of non-isothermal data are based on the rate equation [18, 19]:

$$\frac{d\alpha}{dt} \equiv \beta\frac{d\alpha}{dT} = Af(\alpha)\exp\left(\frac{E_\alpha}{RT}\right) \quad (1)$$

(where α is the conversion, $f(\alpha)$ is the differential conversion function, $\beta = dT/dt$ = const. is the linear heating rate in K min^{-1}, A is the pre-exponential factor in min^{-1}, T is temperature in K, R is the gas constant, E_α is the activation

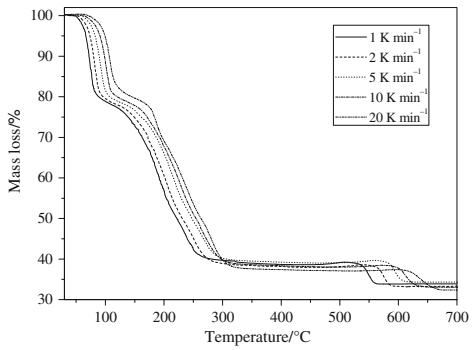

Fig. 5 TG curves for degradation of ammonium niobium oxalate in air atmospheres at different heating rates

energy in kJ mol^{-1}). The subscript α indicates the values related to a particular extent of conversion.

In the constant condition of other parameters, the TG curves for decomposition of ammonium niobium oxalate at various heating rates (β = 1, 2, 5, 10 and 20 K min^{-1}) are shown in Fig. 5. The basic data (β, α, T) are taken from the TG curves.

Two typical isoconversional methods of integral Ozawa–Flynn–Wall and differential Friedman have been widely applied to estimate the apparent activation energy without having to presuppose a certain kinetic model. OFW method is in fact a "model-free" method which assumes that the conversion function $f(\alpha)$ does not change with the variation of the heating rate for all values of degree of conversion α. It involves measuring the temperatures corresponding to fixed values of α from experiments at different heating rates β. Therefore, plotting ln β against $1/T$ in the form of

$$\ln \beta = \log\left[\frac{0.0048AE_\alpha}{g(\alpha)R}\right] - 1.0516\frac{E_\alpha}{RT_\alpha} \quad (2)$$

where $g(\alpha) = \int_0^\alpha f(\alpha)^{-1}\mathrm{d}\alpha$ is the integral conversion function should give a straight line whose slope is directly proportional to the activation energy ($-1.0516E_\alpha/R$).

Friedman proposed the use of the logarithm of the conversion rate dα/dt as a function of the reciprocal temperature, in the form of

$$\ln\left(\frac{\mathrm{d}\alpha}{\mathrm{d}T}\right)_\alpha = \ln[Af(\alpha)] - \frac{E_\alpha}{RT_\alpha} \quad (3)$$

It is obvious from Eq. 3 that if the function $f(\alpha)$ is constant for a particular value of α, then dα/dt is also constant. By plotting ln(dα/dt) against $1/T$, the value of the $-E_\alpha$/R for a given value of α can be directly obtained. Using this equation, it is possible to obtain values for E_α over a wide range of conversions.

OFW plots for the dehydration step of the complex at different α ($0.2 \leq \alpha \leq 0.8$) are exhibited in Fig. 6.

For three decomposition stages, the apparent activation energy can be calculated at different extent of conversion ($0.2 \leq \alpha \leq 0.8$) using both Eqs. 2 and 3, and the results are presented in Figs. 7 and 8, respectively.

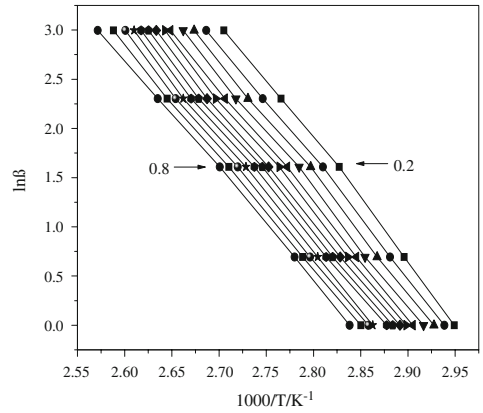

Fig. 6 OFW analysis of the thermal decomposition of ammonium niobium oxalate for the first step at 1, 2, 5, 10, 20 K min^{-1}

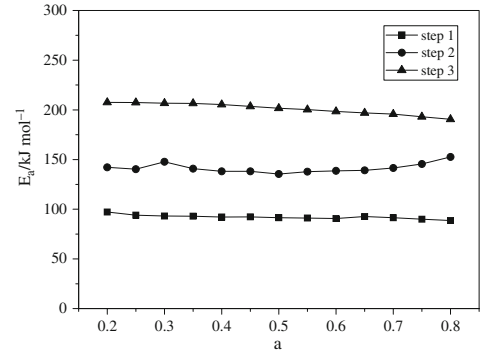

Fig. 7 Apparent activation energy in relation to the conversion for the three steps based on the OFW method

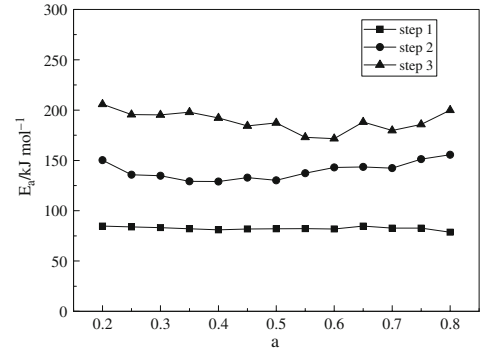

Fig. 8 Apparent activation energy in relation to the conversion for the three steps based on the FR method

It is well known that Friedman method is very sensitive to experimental noise, and tends to be numerically unstable because of employing instantaneous rate value. But OFW method produces a systematic error in E_α when the activation energy varies with α. This error does not appear in Friedman method [20, 21]. It is shown from Figs. 7 and 8 that the activation energies calculated by OFW method are higher than those of Friedman method. It is due to that

Table 2 Non-isothermal kinetic parameters obtained from Coats–Redfern equation and Achar–Bridly–Sharp equation for $\beta = 1$ K min^{-1}

Function no.	C–R				ABS			
	E/kJ mol^{-1}	ln A/s^{-1}	r	SD	E/kJ mol^{-1}	ln A/s^{-1}	r	SD
1	201.23	59.95	−0.9873	0.1412	130.36	42.07	−0.8946	0.2838
2	226.25	68.29	−0.9916	0.1283	174.39	57.05	−0.9498	0.2505
3	56.14	9.10	−0.9928	0.0295	16.05	2.04	−0.4347	0.1449
4	237.79	71.77	−0.9921	0.1311	46.99	13.86	−0.7928	0.1575
5	59.90	10.30	−0.9947	0.0271	29.30	6.54	0.6939	0.1326
6	256.83	77.79	−0.9954	0.1080	226.24	73.97	−0.9793	0.2037
7	236.36	70.43	−0.9931	0.1214	192.20	61.87	−0.9633	0.2336
8	176.04	48.57	−0.9827	0.1447	98.08	28.24	−0.8364	0.2802
9	363.64	116.26	−0.8029	1.1771	328.35	110.27	−0.9961	0.1267
10	31.13	0.35	−0.9966	0.0112	18.35	2.89	−0.6152	0.1025
11	42.53	4.59	−0.9945	0.0195	30.64	7.42	−0.7864	0.1049
12	53.26	8.52	−0.9971	0.0178	40.48	11.00	−0.8553	0.1069
13	66.67	13.37	−0.9950	0.0291	55.23	16.31	−0.9097	0.1099
14	90.81	22.00	−0.9952	0.0388	79.82	25.08	−0.9494	0.1152
15	102.88	26.29	−0.9953	0.0437	92.11	30.01	−0.9595	0.1179
16	141.77	40.04	−0.9974	0.0444	128.99	42.45	−0.9757	0.1263
17	211.50	64.47	−0.9956	0.0873	202.75	68.30	−0.9869	0.1442
18	289.28	91.65	−0.9975	0.0887	276.50	94.04	−0.9910	0.1632
19	436.80	142.96	−0.9976	0.1330	424.02	145.34	−0.9940	0.2031
20	584.31	194.14	−0.9976	0.1773	571.53	196.52	−0.9952	0.2445
21	−205.65	−63.47	−0.8252	0.1627	25.50	7.22	−0.8452	0.0703
22	20.13	−4.00	−0.9801	0.0178	−50.75	−21.65	0.7933	0.1698
23	28.75	−0.71	−0.9827	0.0236	−42.12	−18.43	0.7241	0.1749
24	46.00	5.63	−0.9848	0.0354	−24.87	−12.15	0.5050	0.1853
25	97.74	24.00	−0.9865	0.0707	−76.62	−29.07	0.9074	0.1547
26	149.49	42.04	−0.9870	0.1060	78.61	24.17	−0.8075	0.2503
27	304.72	94.90	−0.9875	0.2118	130.36	42.07	−0.8946	0.2838
28	129.45	34.18	−0.9959	0.0516	103.46	31.99	−0.9503	0.1478
29	110.88	28.40	−0.9916	0.0632	94.95	29.25	−0.9363	0.1552
30	125.54	34.15	−0.9952	0.0540	94.95	30.35	−0.9363	0.1552
31	118.02	30.72	−0.9935	0.0588	77.93	23.61	−0.8939	0.1704
32	118.02	31.41	−0.9935	0.0588	77.93	24.30	−0.8939	0.1704
33	66.49	13.14	−0.9627	0.0814	−75.25	−29.45	0.7212	0.3150
34	45.06	5.46	−0.9272	0.0793	−177.36	−65.34	0.8813	0.4146
35	30.48	0.07	−0.8817	0.0711	−279.48	−101.35	0.9211	0.5150
36	96.37	25.06	−0.9720	0.1016	231.10	78.75	−0.9974	0.0730
37	199.86	61.01	−0.9980	0.0546	233.10	79.75	−0.9935	0.0960
38	45.32	6.15	−0.9686	0.0507	180.05	59.90	−0.9935	0.0898
39	−200.31	−60.35	−0.9012	0.3982	−76.62	−29.07	0.9074	0.1547
40	−70.62	−27.07	0.90568	0.2046	−76.62	−28.38	0.9075	0.1546
41	198.49	62.08	−0.9735	0.2032	333.22	115.74	−0.9964	0.1240

Friedman method is very sensitive to experimental noise, but OFW method leads to meaningful result assuming that E_α invaries with α, which is just for OFW method. The approximately constant value of E_α for α also suggests that the rate-limiting step of each reaction probably obey a single kinetic mechanism [22, 23].

Lin et al. [24] calculated the average activation energies for the decomposition of nickel oxalate and magnesium oxalate are 205.72 and 152.60 kJ mol^{-1} by OFW methods, respectively. While the average activation energy for the decomposition of ammonium niobium oxalate is about 139.62 kJ mol^{-1}. Dollimore et al. [25] showed that there is a decrease in decomposition temperature with increase in the ionic radius. The radius of Nb(V) (7.0 nm) is bigger than that of Ni(II) (6.9 nm) and Mg(II) (6.5 nm) and based on Coulombic attraction, the Nb(V) will have a weaker metal–oxygen bond (M–O bond) than that of Ni(II) and Mg(II). A decrease in M–O bond strength would, thus lead to a decrease in decomposition temperature. Moreover, the effect of activation energy of the decomposition cannot be ignored.

Determination of the most probable kinetic model

In order to confirm the exact mechanism in each stage, mathematical analysis was performed by the modified Coats–Redfern integral method and Achar–Bridly–Sharp differential method.

$$\text{Coats-Redfern Eq.}: \quad \ln\left[\frac{g(\alpha)}{T^2}\right] = \ln\left[\frac{AR}{\beta E}\right] - \frac{E}{RT} \tag{4}$$

The values of E, $\ln A$ and the linear correlation coefficients r are calculated from the linear least-squares plot of $\ln[g(\alpha)/T^2]$ vs. $1/T$, which the slope is equal to $-E/R$ and the intercept is equal to $\ln(AR/\beta E)$.

$$\text{Achar-Bridly-Sharp Eq.}: \quad \ln\left[\frac{1}{f(\alpha)}\frac{\mathrm{d}\alpha}{\mathrm{d}t}\right] = \ln(A/\beta) - \frac{E}{RT} \tag{5}$$

Plotting $\ln\{[1/f(\alpha)][\mathrm{d}\alpha/\mathrm{d}t]\}$ vs. $1/T$, a straight line is given. The activation energy E and $\ln A$ can be obtained from the slope $-E/R$ and the intercept $\ln(A/\beta)$.

The basic data α, T and $\mathrm{d}\alpha/\mathrm{d}t$ of the three decomposition steps and forty-one reaction models [26] were inserted into Eqs. 4 and 5. When the values of E and $\ln A$ obtained by the two methods are approximately equal with those of OFW and Friedman methods and the linear correlation coefficient is higher, it can be concluded the relevant function is the probable mechanism.

For the first step of dehydration, the results and the reaction function number are listed in Table 2. Comparing the activation energies data in Table 2, the possible kinetics models and respective kinetic parameters at various heating rates are tabulated in Table 3.

From Table 3, we can see that function 14, namely, $g(\alpha) = (3/2)(1-\alpha)\ln(1-\alpha)^{2/3}$ and $f(\alpha) = (3/2)(1-\alpha)\ln(1-\alpha)^{1/3}$, is the most probable mechanism function of the dehydration of ammonium niobium oxalate. Therefore, the first stage of the decomposition mechanism is controlled by assumed random nucleation and its subsequent growth (Avrami-Eerofeevn, $n = 2/3$). Function 19 (Avrami-Eerofeevn, $n = 3$), namely, $g(\alpha) = \ln(1-\alpha)^3$ and $f(\alpha) = (1/3)(1-\alpha)[-\ln(1-\alpha)]^{-2}$, is the most probable mechanism function of the decomposition of ammonium niobium oxalate.

However, no reasonable kinetic model can be obtained for the third step by means of above model-fitting methods. The results suggest that the third step could not be interpreted by the forty-one reaction models in this study, or the thermal decomposition step could be multi-step kinetics [27].

Table 3 The kinetics parameters from differential method and integral method for the possible kinetic models at the five heating rates

Stage	β/K min^{-1}	Function no.	C–R			ABS		
			E/kJ mol^{-1}	ln A/s^{-1}	r	E/kJ mol^{-1}	ln A/s^{-1}	r
Step 1	1	14	90.81	22.00	−0.9952	79.82	25.08	−0.9494
	2	14	87.29	20.06	−0.9975	85.45	27.00	−0.9899
	5	14	79.58	16.58	−0.9979	80.76	25.47	−0.9851
	10	14	77.75	15.29	−0.9977	83.70	26.37	−0.9927
	20	14	79.28	15.22	−0.9962	71.49	22.52	−0.9238
Step 2	1	19	142.45	25.82	−0.9955	130.39	32.47	−0.9921
	2	19	143.34	25.24	−0.9941	131.64	32.70	−0.9909
	5	19	151.31	26.18	−0.9951	138.56	34.41	−0.9931
	10	19	149.21	25.05	−0.9980	143.77	35.81	−0.9949
	20	19	138.05	21.77	−0.9989	129.79	32.55	−0.9966

Conclusions

This work synthesized ammonium niobium oxalate and determined the molecular formula as $NH_4(NbO(C_2O_4)_2(-H_2O)_2)(H_2O)_3$. According to TG measurements, the thermal decomposition of ammonium niobium oxalate occurs in three steps. Based on model-free method, the apparent activation energies for the three steps are calculated. For the model-fitting method, the most probable kinetic model of the first step decomposition is described by Avrami-Eerofeevn, $n = 2/3$, while the second one is fitted by Avrami-Eerofeevn, $n = 3$.

References

1. Nowak I, Ziolek M. Niobium compounds: preparation, characterization, and application in heterogeneous catalysis. Chem Rev. 1999;99:3603–24.
2. Wang W, Li J, Li H, Lu D, Mi XX, Zhong M, Liu J. The preparation of niobium oxalate. CN patent, CN1935772, 2007.
3. Narendar Y, Messing GL. Synthesis, decomposition and crystallization characteristics of peroxo-citrato-niobium: an aqueous niobium precursor. Chem Mater. 1997;9:580–7.
4. Ziolek M. Niobium-containing catalysts – the state of the art. Catal Today. 2003;78:47–64.
5. Galwey AK, Mohamed MA. Kinetic and thermodynamic studies of the nonisothermal decomposition of anhydrous copper(II) formate in different gas atmospheres. Thermochim Acta. 1993; 213:279–91.
6. Mohamed MA, Galwey AK. Kinetic and mechanistic study of the isothermal decomposition of ferric oxalate dihydrate. Thermochim Acta. 1993;213:269–78.
7. Mohamed MA, Galwey AK. A kinetic and mechanistic study of the thermal decomposition of copper(II) oxalate. Thermochim Acta. 1993;217:263–7.
8. Mohamed MA, Halawy SA, Salem MA. Non-isothermal decomposition of potassium ferrioxalate trihydrate. J Anal Pyrolysis. 2000;55:55–67.
9. Macklen ED. Influence of atmosphere on the thermal decomposition of ferrous oxalate dehydrate. J Inorg Nucl Chem. 1967;29: 1229–34.
10. Blodyrev VV, Nev'yantsev IS, Mikhailov YI, Khairetdinov EF. On the mechanism of thermal decomposition of oxalates. Kinet Katal. 1970;11(2):367–73.
11. Viswanathan B, Gopalakrishnan J, Srinivasan V, Sastri MVC. Thermal decomposition of hydrated iron(II) oxalate and manganese(II) oxalate in vacuum. J Therm Anal. 1971;3:429–31.
12. Ozawa T. A new method of analyzing thermogravimetric data. Bull Chem Soc Jpn. 1965;38:1881–6.
13. Friedman HL. Kinetics of thermal degradation of char-forming plastics from thermogravimetry. J Polym Sci Part C. 1964;61: 183–95.
14. Coats AW, Redfern JP. Kinetic parameters from thermogravimetric data. Nature. 1964;201:68–9.
15. Achar BN. Thermal decomposition kinetics of some new unsaturated polyesters. J Proc Int Clay Conf. 1969;1:6.
16. Braga VS, Dias JA, Dias SCL, Macedo JL. Catalyst materials based on Nb_2O_5 supported on SiO_2-Al_2O_3: preparation and structural characterization. Chem Mater. 2005;17:690–5.
17. Saha B, Ghoshal AK. Model-free kinetics analysis of ZSM-5 catalyzed pyrolysis of waste LDPE. Thermochim Acta. 2007;453: 120–7.
18. Guinesi LS, Ribeiro CA, Crespi MS, Veronezi AM. Tin(II)-EDTA complex: kinetic of thermal decomposition by non-isothermal procedures. Thermochim Acta. 2004;414:35–42.
19. Jankovic B, Mentus S. Model-fitting and Model-free analysis of thermal decomposition of palladium acetylacetonate [$Pd(acac)_2$]. J Therm Anal Calorim. 2008;94(2):395–403.
20. Zhang J, Zeng JL, Liu YY, Sun LX, Xu F, You WS, et al. Thermal decomposition kinetics of the synthetic complex Pb(1,4-BDC) (DMF)(H_2O). J Therm Anal Calorim. 2008;91(1):189–93.
21. Vyazovkin S. Modification of the integral isoconversional method to account for variation in the activation energy. J Comput Chem. 2001;22:178–83.
22. Tita B, Marian E, Tita D, Vlase G, Doca N, Vlase T. Comparative kinetic study of decomposition of some diazepine derivatives under isothermal and non-iso-thermal conditions. J Therm Anal Calorim. 2008;94(2):447–52.
23. Gabal MA. Non-isothermal studies for the decomposition course of CdC_2O4–ZnC_2O_4 mixture in air. Thermochim Acta. 2003;402: 199–208.
24. Lin CM, Chen DH, Tang WJ. Synthesis of $MgNi_2O_3$ and kinetics of thermal decomposition of the oxalate precursor. J Anal Appl Pyrolysis. 2006;75:240–4.
25. Dollimore D, Griffith DL, Nicholson D. The thermal decomposition of oxalates: part II. Thermogravimetric analysis of various oxalates in air and in nitrogen. J Chem Soc. 1963;2707–11.
26. Hu RZ, Shi QZ. Thermal analysis kinetics. Beijing: Science Press; 2001.
27. Vyazovkin S. Model-free kinetics: staying free of multiplying entities without necessity. J Therm Anal Calorim. 2006;83:45–51.